ESA Climate Change Initiative – Fire_cci

O3.D3 Intermediate validation results: SAR pre-processing and burned area detection

Project Name	ECV Fire Disturbance: Fire_cci Phase 2
Contract №	4000115006/15/I-NB
Issue Date	25/01/2018
Version	1.0
Author	Mihai A. Tanase, Miguel Angel Belenguer Plomer
Document Ref.	Fire_cci_O3.D3_Int.Val.-SFD-SA_v1.0
Document type	Internal

Project Partners

Prime Contractor/ Scientific Lead & Project Management	UAH – University of Alcala (Spain)
Earth Observation Team	UAH – University of Alcala (Spain) EHU – University of the Basque Country (Spain) UL – University of Leicester (United Kingdom) UCL – University College London (United Kingdom) ISA – School of Agriculture, University of Lisbon (Portugal)
System Engineering	BC – Brockmann Consult GmbH (Germany)
Climate Research Group	MPIC – Max Planck Institute for Chemistry (Germany) IRD - Research Institute for Development (France) LSCE - Climate and Environmental Sciences Laboratory (France) VUA - Stichting VU-VUmc (Netherlands)

Distribution

Affiliation	Name	Address	Copies
ESA	Stephen Plummer (ESA)	stephen.plummer@esa.int	electronic copy
Project Team	Emilio Chuvieco (UAH)	emilio.chuvieco@uah.es	electronic copy
	M. Lucrecia Pettinari (UAH)	mlucrecia.pettinari@uah.es	
	Joshua Lizundia (UAH)	joshua.lizundia@uah.es	
	Gonzalo Otón (UAH)	gonzalo.oton@uah.es	
	Mihai Tanase (UAH)	mihai.tanase@uah.es	
	Miguel Ángel Belenguer (UAH)	miguel.belenguer@uah.es	
	Aitor Bastarrika (EHU)	aitor.bastarrika@ehu.es	
	Ekhi Roteta (EHU)	ekhi.roteta@gmail.com	
	Kevin Tansey (UL)	kjt7@leicester.ac.uk	
	Marc Padilla Parellada (UL)	mp489@leicester.ac.uk	
	James Wheeler (UL)	jemw3@leicester.ac.uk	
	Philip Lewis (UCL)	ucfalew@ucl.ac.uk	
	José Gómez Dans (UCL)	j.gomez-dans@ucl.ac.uk	
	James Brennan (UCL)	james.brennan.11@ucl.ac.uk	
	Jose Miguel Pereira (ISA)	jmocpereira@gmail.com	
	Duarte Oom (ISA)	duarte.oom@gmail.com	
	Manuel Campagnolo (ISA)	mlc@isa.ulisboa.pt	
	Thomas Storm (BC)	thomas.storm@brockmann-consult.de	
	Johannes Kaiser (MPIC)	j.kaiser@mpic.de	
	Angelika Heil (MPIC)	a.heil@mpic.de	
	Florent Mouillot (IRD)	florent.mouillot@cefe.cnrs.fr	
	M. Vanesa Moreno (IRD)	mariavanesa.morenodominguez@cefe...	
	Philippe Ciais (LSCE)	philippe.ciais@lsce.ipsl.fr	
	Chao Yue (LSCE)	chaoyuejoy@gmail.com	
	Pierre Laurent (LSCE)	pierre.laurent@lsce.ipsl.fr	
	Guido van der Werf (VUA)	guido.vander.werf@vu.nl	
	Ioannis Bistinas (VUA)	i.bistinas@vu.nl	

Summary

The aim of Option 3 is to provide Sentinel-1 burned area products over a large demonstrator area (LDA) located in tropical South America. This document supplements the deliverable *O3.D1 Algorithm Theoretical Basis Document (ATBD) – Small Fires Dataset (SFD) for the large demonstrator area (LDA) in South America* where the BA algorithm is described.

The document is comprised of three main parts describing preliminary results of the algorithms implemented for SAR pre-processing and burned area detection. The first part describes the evaluation of the SAR pre-processing chain (based on Orfeo ToolBox, OTB) selected for pre-processing the Amazon large demonstrator area (LDA). The OTB chain is evaluated against the Gamma Remote Sensing (GRS) chain. The comparison was necessary as the Burned Area (BA) algorithm was developed using ground range detected (GRD) images pre-processed through the GRS chain available at the start of Option 3. Comparison of the two chains was essential to understand BA algorithm transferability from the development environment (GRS-based) to the cloud environment (OTB-based). The geometry and the radiometry of the output Sentinel-1 imagery were assessed.

The second part of this document focuses on BA algorithm performance as a function of GRD processing chain. The test was carried out over a single processing tile.

The third part of this document describes the preliminary validation of the Burned Area (BA) algorithm as well as the processing speed and accuracy at two different spatial resolutions (20 and 40 m). The preliminary validation was carried out over five tiles using reference burned areas generated from Landsat 8 images, as per *O3.D1 Algorithm Theoretical Basis Document (ATBD) – Small Fires Dataset (SFD) for the large demonstrator area (LDA) in South America.* The processing speed and accuracy as a function of spatial resolution was tested over two tiles.

	Affiliation/Function	Name	Date
Prepared	UAH	Mihai A. Tanase	31/10/2017
Reviewed	UAH - Science Leader UAH – Project Manager	Emilio Chuvieco Lucrecia Pettinari	
Authorized	UAH - Science Leader	Emilio Chuvieco	
Accepted	ESA - Technical Officer	Stephen Plummer	

This document is not signed. It is provided as an electronic copy.

Document Status Sheet

Issue	Date	Details
1.0	25/01/2018	First Issue of the document

Document Change Record

Issue	Date	Request	Location	Details

Table of Contents

List of Tables

List of Figures

1 Executive Summary

Option 3 uses the systematically distributed Sentinel-1 Level-1 Ground Range Detected (GRD) data to detect burned area over a large demonstrator area (LDA) located in the Amazon basin. Detailed information on the Sentinel-1 system and the Burned Area (BA) algorithm are available in [RD-2]. This deliverable documents the quality of the selected SAR pre-processing chain and provides the preliminary validation of the BA algorithm developed within Option 3.

A processing chain based on the Orfeo ToolBox (OTB) was selected to pre-process Sentinel-1 GRD data over the Amazon LDA. Since the development of the BA algorithm was carried out on GRD data processed through a different pre-processing chain (based on libraries from Gamma Remote Sensing, GRS), there was a need to validate the geometry and radiometry of the two pre-processing chains to ensure their compatibility. Comparison of the two pre-processing chains was based on the outputs from a single test area. As the GRS pre-processing chain was set-up and tested within prior projects, its optimal processing parameters were known. For OTB, different processing parameters were trialled, and the results were tested (geometry and radiometry) against the GRS outputs (i.e. reference). The comparisons show that geometrically, OTB and GRS are closely matched. However, the radiometry of the OTB outputs was different (considerably noisier). The cause was identified as a lack of multi-looking intermediate step when generating lower spatial resolution products. To compensate this, OTB pre-processing was carried out at 20m (native S-1 GRD resolution) and the results were aggregated to 40 m spatial resolution. This post-processing aggregation step was added to the original OTB processing chain.

For BA implementation over large areas, the performance of the algorithm (processing speed and accuracy) needs to be evaluated at different spatial resolutions. The analysis was needed to ensure an optimum selection of the spatial resolution for GRD data pre-processing. A pre-condition of such an evaluation, however, was the selection of the optimum pre-processing chain for GRD data from BA algorithm perspective. To this end, the BA algorithm was evaluated on GRD data processed through both pre-processing chains to ensure that classification results are similar. The results showed that accuracy metrics do not depend on the GRD pre-processing chain with (overall accuracy (OA), Producer and User accuracy) varying marginally. Such small variations constitute further evidence on the compatibility of two GRD pre-processing chains. In terms of speed and consistency, the BA algorithm needed eight times longer to process one tile when the spatial resolution was halved from 40 to 20 m. The accuracy of the classification did not change drastically when working at the two spatial resolutions with OA remaining constant, while variations of ±2-5% were observed for OE and CE. Considering these results, a spatial resolution of 40 m was selected. Such a resolution ensured a balance between BA precision (commission and omission errors) and algorithm processing time.

Once optimum parameters (i.e., spatial resolution) for the BA algorithm were established, the preliminary validation of the BA algorithm was carried out using as set of three independent datasets (MGRS tiles 18NXG, 19LGL, and 20LQQ). The results show average omission and commission errors of 31% and 38% respectively. It is necessary to notice that the reference datasets derived from Landsat are also subjected to errors and that temporal mismatches between Sentinel-1 and the reference data may have further influenced the agreement between the Sentinel-1 detected map and the Optical based reference data.

2 Introduction

2.1 Purpose of the document

The objective of this document is to describe the inter-comparison results between GRS and OTB S-1 pre-processing chains. The document provides a quantitative assessment of the BA algorithm accuracy using independent datasets. This document complements the O3.D1 Algorithm Theoretical Basis Document - ATBD [RD-2].

2.2 Applicable Documents

[RD-1]	Option 3, Radar Burn Ratio for burnt area detection and mapping, Proposal prepared for ESA on September 12, 2016. Option to ECV Fire Disturbance Phase-2 project.
[RD-2]	Algorithm Theoretical Basis Document (ATBD) – Small Fires Dataset (SFD) for the large demonstrator area (LDA) in South America

2.3 Background

The goal of BA detection algorithms is providing information about land cover state. Since inference processes (models) are affected by errors there is an element of uncertainty regarding the results produced using remote sensing data. The quality of the input data influences the ability to detect burned areas. Therefore, the quality of remote sensing data and the derived products needs to be characterized quantitatively to facilitate critical information on product reliability to the end users.

The BA algorithm developed in Option 3 uses temporal time-series of the backscatter coefficient to identify changes and associate them with biomass burning events as described in [RD-2]. The backscatter coefficient gives an indication of the amount of energy that is returned from the surface. The algorithm considers multi-temporal changes of incoherent SAR-based metrics (e.g. backscattering coefficient intensities). For an efficient BA detection, the SAR processing chains need to provide multi-temporal series of co-located pixels (very accurate geometry) as well as low pixel-wide noise needed for change detection and classification. Therefore, SAR pre-processing outputs need to be evaluated for spatial accuracy and consistency as well as radiometric quality (noise levels).

Algorithm deployment over large areas is conditioned by its performance (speed) and accuracy. Both parameters are influenced by the spatial resolution to which products are processed as omission and commission errors are highly depended on the pixel size and the processing speed increases linearly with decreasing pixel size. Therefore, assessing the effect of spatial resolution on processing times and product accuracy metrics was essential for selecting the optimum pixel size for BA algorithm deployment. Accuracy of the results was characterized through cross-tabulation against reference datasets, not used during the BA algorithm development, by accounting for the spatio-temporal coincidences and disagreements. The approach is widely used in BA mapping projects. (Boschetti et al. 2004; Boschetti et al. 2016; Chuvieco et al. 2008; Giglio et al. 2009; Padilla et al. 2014; Padilla et al. 2017; Roy and Boschetti 2009). The reference maps are derived from medium spatial resolution images (Lansdat 8) using the Burned Area Mapping Software (BAMS) as described in [RD-2]. One should bear in mind that cross-tabulation based on ancillary reference datasets derived from remote sensing data

acquired by other sensors, largely indicates the agreement between BA products as the accuracy of the reference dataset is not known. In addition, mismatches between sensors passes may results in disagreements of the detected burned area due to the different acquisition dates.

3 Sentinel-1 pre-preprocessing

Option 3 uses the systematically distributed Level-1 Ground Range Detected data which need further processing to allow for burned area detection. To fulfill the requirements of the BA algorithm, multi-temporal series of co-located pixels and low pixel-wide noise, two SAR data pre-processing chains were compared: 1) the Gamma Remote Sensing (GRS), and 2) Orfeo ToolBox (OTB) pre-processing.

The OTB chain was developed at the Centre of the Study of the Biosphere from Space (CESBIO) and is distributed (since April 2017) under an open access General Public License (GPL). The proprietary GRS SAR pre-processing chain was used for GRD data pre-processing in areas selected for BA algorithm development as it was available at the start of Option 3 (October 2016). The two chains share a similar approach with major differences regarding the output geometry, orbital strips for GRS and tiles (100 km Military Grid Reference System) for OTB. A further difference is the existence of a co-registration step in the GRS chain. As Sentinel-1 orbital vector information is highly accurate the co-registration step was deemed unnecessary in the OTB pre-processing chain. Since the BA algorithm considers multi-temporal changes of incoherent SAR-based metrics (i.e. backscattering coefficient intensities) the geometry (co-located pixels) and radiometry (noise level) of the pre-processed GRD images are of crucial importance. Precisely co-located temporal stacks of pixels are needed to ensure that detected multi-temporal changes are not caused by spatial miss-registration. At the same time, low noise levels (~100 equivalent number of looks, or ENL) are needed when mapping land cover at pixel level (Quegan et al. 2000). Noise reduction may be achieved through spatial aggregation (multi-looking) or multi-temporal filtering (MTF). As multi-looking reduces the spatial resolution of the output products it is often combined with MTF to achieve the required ENL and preserve higher spatial resolution of the SAR data. This latter approach is preferred when sufficient multi-temporal datasets are available.

3.1 GRS pre-processing chain

The GRS SAR pre-processing chain is automatized through MATLAB scripting. Data processing includes various steps which might be summarized as pre-processing, co-registration, and geo-referencing (Figure 1).
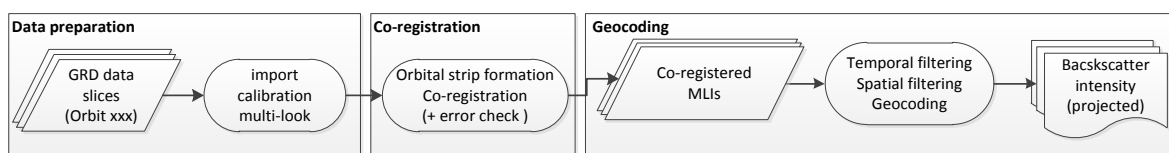
Figure 1: Flowchart for SAR data processing with Gamma Remote Sensing

Data preparation: processing starts by organizing GRD data into relative orbits. Processing parameters are also set: output spatial resolution, the type of filtering (spatial and/or temporal), the desired co-registration method, as well as the use of topographic normalization. GRD data are extracted and imported into a format readable by the Gamma Software using the information provided in the annotation files (metadata,

calibration, and noise). Checks are included to ensure images from the same relative orbital path are processed within a given run. The result is a multi-looked image (MLI) in slant range geometry accompanied by a parameter file describing its properties (e.g. acquisition date/time, range and azimuth resolutions, orbital state vectors).

Co-registration: MLI data slices are assembled to form the original orbits prior to co-registration and the state vectors are updated using precise orbit determination (POD). Strips of MLI data, acquired from the same orbital path are co-registered using as reference the first image of the data series. Offsets with respect to the reference image are automatically collected for the remaining (slave) images using a cross-correlation algorithm (Werner et al. 2005). MLI slave strips are re-sampled to the geometry of the reference image (master). By default, each image is multi-looked in range and azimuth to obtain a ground pixel spacing of approximately 50 m (the spatial resolution desired for the subsequent analysis). During multi-looking MLI strips are re-calibrated to the normalized radar cross-section gamma-naught backscatter coefficient.

Geocoding: is based on a lookup table describing the transformation between the radar and the map geometry (Wegmüller et al. 2002). The lookup table is generated using the Shuttle Radar Topography Mission (SRTM) digital elevation model (DEM) and the orbital information of the SAR sensor. Each MLI strip is topographically normalized to correct for the radiometric distortions introduced by the rough topography, the varying incidence angle from near to a far range and the effective pixel surface (Frey et al. 2013). Multi-temporal filtering (1) is applied to further reduce speckle while preserving spatial resolution after multi-looking (Quegan et al. 2000). The lookup table is subsequently used to transform the normalized, multi-temporal filtered MLI images (master and slaves) to the cartographic projection of the DEM used to generate the lookup table.

$$J_k(x,y) = \frac{E[I_k]}{N} \sum_{i=1}^{N} \frac{I_i(x,y)}{E[I_i]} \tag{1}$$

Where N is the number of co-registered images, intensity in the *k*th image at position *(x,y)* is denoted by $I_k(x,y)$ and $E[I]$ is the local mean value of pixels in a window centered at *(x,y)* in image *I*.

3.2 OTB pre-processing chain

The Sentinel-1 OTB chain is the tool for Sentinel-1 GRD data tiling and processing to the 100 km MGRS tiles used by the Sentinel-2 processing system. The chain is highly scalable (multithreading/multiprocessor) and autonomous once few parameters are set. The chain also deals with data download from the PEPS (*Plateforme d'Exploitation des Produits Sentinel*) repository that mirrors ESA's Scihub. S1-OTB processing may be grouped in several steps, pre-processing, and geo-referentiation and temporal filtering (Figure 2).
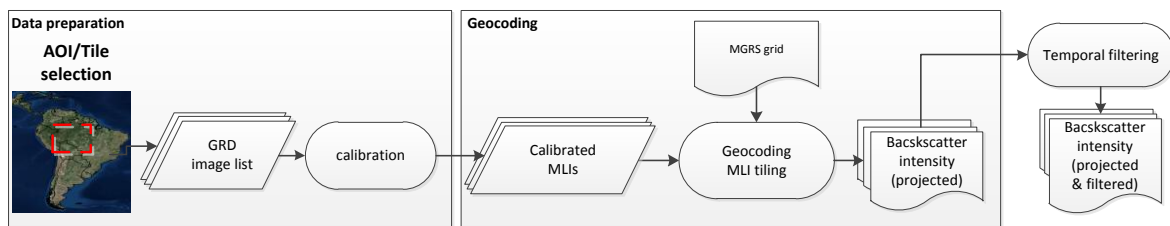

**Figure 2: Flowchart for SAR data processing with OTB**

	Fire_cci	Ref.:	Fire_cci_O3.D3_Int.Val.-SFD-SA_v1.0		
	Intermediate validation results: SAR pre-	Issue	1.0	Date	25/01/2018
	processing and burned area detection	Page			10

The pre-processing steps includes data download (ascending and descending passes) according to the specified MGRS tiles and calibration to gamma or sigma nought. The geocoding step includes orthorectification to the desired spatial resolution, data subset to the current processing tile as well as slice assembly for data acquired from the same orbital path but provided within different slices. The last step is multi-temporal filtering of the products according to satellite pass. Compared to GRS, the OTB chain is characterized by lacking the co-registration and multi-looking steps, which may have influence on the output geometry and respectively radiometry.

4   GRS vs. OTB: S1 pre-processing inter-comparison

4.1   Geometry

Comparison of outputs from the two processing chains were carried out over one MGRS tile (49MGT) located in a tropical forest in the island of Borneo, Indonesia (Figure 3). The area was selected as it was previously used within other projects (Tanase et al. 2015). This area also lays within Fire_cci RSS special case study on fire emissions.
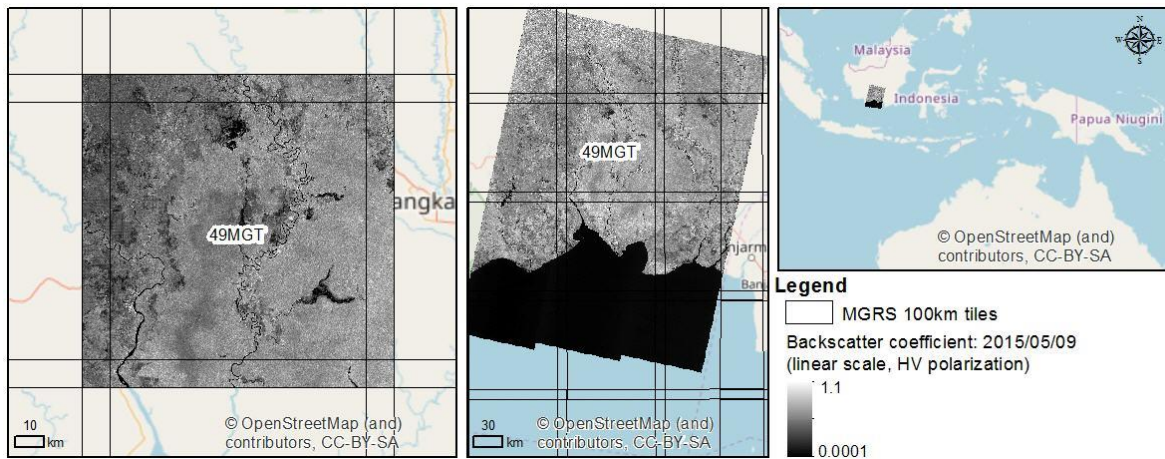
Figure 3: Area used for GRS vs. OTB pre-processing inter-comparison. The left panel shows OTB output for tile 49MGT. The center panel shows GRS output for relative orbit 3 descending (3D) which includes the area covered by tile 49MGT shown in the left panel

Output geometry of GRS and OTB products correspond at pixel level for the same spatial resolution (Figure 4). Such correspondence was expected as both processing chains use the orbital state vectors during orthorectification. The results confirm the redundancy of co-registration step which may be safely switched off when using the GRS processing chain (i.e., shorter processing time). One should notice that the output geometry analysis was not geared towards demonstrating the absolute geolocation accuracy of the Sentinel-1 products since such studies already exist (Schubert et al. 2015). The multi-temporal analysis of the OTB outputs' geometry shows pixel level correspondence (Figure 5), confirming the multi-temporal stability of the orbital state vectors. As such, temporal changes detected through the BA algorithm can be considered genuine changes due to a changed scattering process and not due to miss-registration errors.

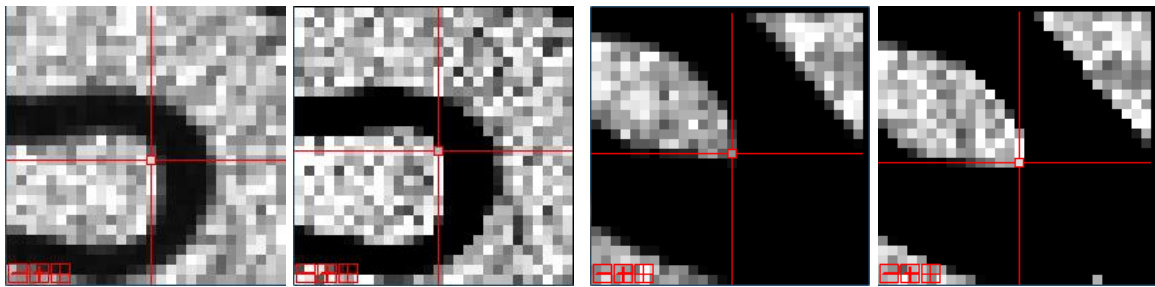|	**Fire_cci**	Ref.:	Fire_cci_O3.D3_Int.Val.-SFD-SA_v1.0	
	Intermediate validation results: SAR pre-	Issue	1.0	Date	25/01/2018
	processing and burned area detection	Page		11	

Figure 4: Spatial correspondance between GRS (left) and OTB (right) outputs at two locations. SAR image acquired on 2015/05/09. Red crosses shows the coordinates of the geo-linked outputs.
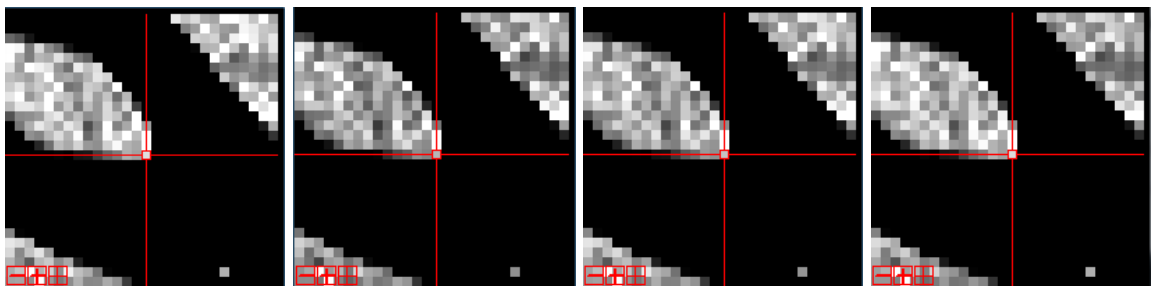

Figure 5: Multi-temporal spatial correspondance of OTB outputs at 50 m resolution. From left to right, SAR images acquired on 2015/05/09, 2015/06/02, 2015/06/26, and 2015/07/20. Red crosses shows the same coordinates of the geo-linked OTB outputs.

4.2   Radiometry

Outputs radiometry was analyzed by comparing the equivalent number of looks (ENL). ENL is an important parameter in statistical modeling of multi-look synthetic aperture radar (SAR) images. ENL describes the degree of averaging applied to the SAR measurements during data formation and post-processing (Anfinsen et al. 2009). Multi-looking is required to moderate speckle (noise like interference), a characteristic of all coherent imaging systems, and takes place either in the frequency domain or as a post-processing operation (after SAR focusing). In this process, correlated measurements are averaged. The ENL describes the number of independent measurements out of the total number of the correlated samples averaged. ENL influences the accuracy of the information from multi-looked SAR data and its values are needed particularly for applications focused on pixel-level classification and change detection (Quegan et al. 2000).

The ENL, computed as the ratio between the squared mean backscatter and the squared standard deviation, is commonly estimated by identifying homogeneous regions in an image, where the speckle is fully developed, and contribution of texture is negligible, meaning that the radar cross section is assumed to be constant (Anfinsen et al. 2009). Such conditions are often encountered over homogeneous forests, with undisturbed tropical forest being particularly suitable as environmental conditions are largely stable. Therefore, ten homogeneous areas (600 to 10.000 ha polygons) have been selected within tropical forests located in the 49MGT MGRS tile (Figure 6) and used for ENL computation. The ENL value was computed for each polygon and then averaged. Table 1 shows the average ENL value for different OTB outputs depending on the selected processing parameters. For comparison it also shows the ENL values of the GRS outputs. One should notice that both, GRS and OTB processing chains were applied over the same

	Fire_cci	Ref.:	Fire_cci_O3.D3_Int.Val.-SFD-SA_v1.0
	Intermediate validation results: SAR pre-	Issue	1.0	Date	25/01/2018
	processing and burned area detection	Page			12

temporal period (2015/05/01 to 2015/12/30) to avoid influencing the results of the multi-temporal filtering algorithm which depends on the number of input images. OTB processing was carried out at different spatial resolutions (10, 20, 30 and 50 m) and using with different spatial filtering windows (5, 7, 9 pixels wide). GRS processing was carried out at a fixed (50m) spatial resolution and the ENL was compared for two types of data (unfiltered and temporally filtered).
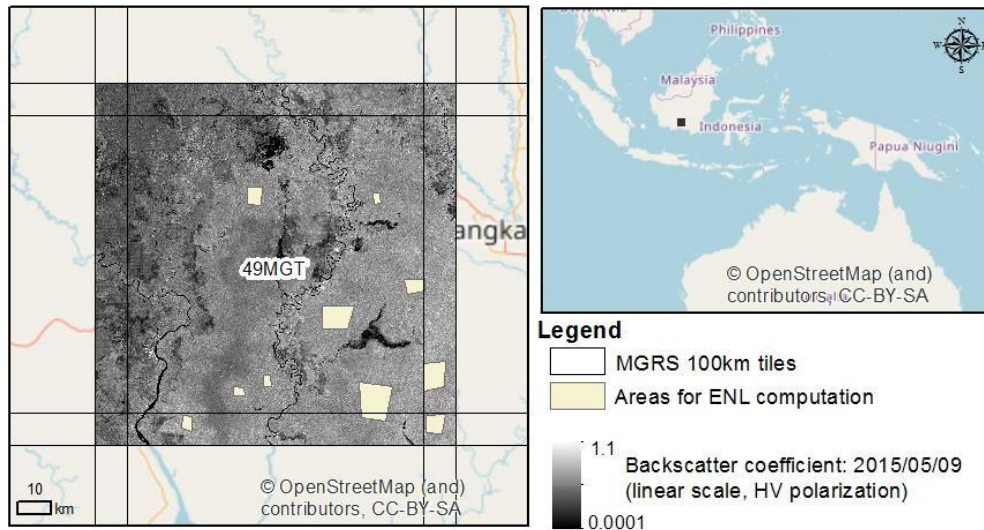
Figure 6: Area used for the computation of the Equivalent Number of Looks (ENL).

Table 1: The Equivalent Number of Looks (ENL) as a function of processing parameters and filtering windows for S1 images process through OTB and GRS pre-processing chains. Results for tile 49MGT, Borneo, Indonesia. GRD data acquired between 2015/05/01 and 2015/12/30 were used for multi-temporal filtering. ENL computed for the image acquired on 2015/05/09. In grey, aggregated products.

Processing chain	Processing parameters		ENL
	Spatial resolution (m)	**Filtering window (pixels)**	
OTB	10	7	24.8
	20[1]	NA	23.5
	50[2]	NA	80.1
	20	7	27.5
	40[1]	NA	70.0
	30	5	27.3
	30	7	27.9
	30	9	28.2
	50	5	27.2
	50	7	27.7
	50	9	28.0
GRS	50	unfiltered	29.7
	50	3	73.6
	50	additive*	81.4

* pre-filtered images (Frost filter, 3 pixels window size) are used to compute the local statistics needed for multitemporal filtering.
[1] Aggregated product starting from the 10m output
[2] Aggregated product starting from the 20m output

Table 1 shows the small difference in ENL (~3.5) between OTB products processed at increasing spatial resolutions (10, 20, 30, and 50m) as well as the marginal difference (<1) between OTB products processed at the same spatial resolution (30 or 50m), but

	Fire_cci	Ref.:	Fire_cci_O3.D3_Int.Val.-SFD-SA_v1.0
	Intermediate validation results: SAR pre-	Issue	1.0	Date	25/01/2018
	processing and burned area detection	Page	13

using different filtering windows sizes. At the same time, the GRS MTF product shows a significantly larger ENL (73.6) as opposed to ENL values between 25 and 28 for the OTB MTF outputs.

The large discrepancy was attributed to a missing multi-looking step before orthorectification for the OTB pre-processing chain. The lack of multi-looking results in resampling noisier, high-resolution SAR data to lower spatial resolutions. Without prior multi-looking, the added benefit of speckle reduction is lost. A workaround, addressing the OTB pre-processing lack of multi-looking, was implemented in the form of 1) SAR data processing at a spatial resolution of 20m (the full resolution of Level-1 GRD products) followed by 2) pixel aggregation (multi-looking in the spatial domain) of the MTF images to 40 m resolution. Indeed, after applying the solution above, the ENL of GRS and OTB were more similar (81.4 vs 80.1). Notice that direct comparisons of ENL from temporally unfiltered data with ENL of temporally filtered data does not provide meaningful results.

5   GRS vs. OTB: BA inter-comparison

To understand the effect of SAR data pre-processing chain on BA detection accuracy, the algorithm described in [RD-2] was applied over one validation tile (20LQQ) processed through GRS and the OTB chains (Figure 7). Overall accuracy (OA), commission (CE), and omission (OE) errors were computed with respect to the burned area detected from Landsat 8 (Path/Frame 230/066). Eight Sentinel 1 images were available for April to October period albeit one (20.08.2016) was not processed with the GRS chain (Table 2). Seven Landsat images (Path/Row 233/066) with cloud cover below 30% were available between May and September 2016 over the same area (Table 2). The difference in burned area OA for Sentinel-1 data processed through OTB and GRS chains was rather small (3%). The difference in omission errors was slightly higher (7%) with OTB chain showing the better results. The much lower commission errors observed for the OTB chain may be linked to the availability of one more data (20.08.2016 image) during the analyzed period, thus maintaining the frequency of Sentinel 1 datasets to at least one per month (notice the 12 weeks gap between July 3rd and September 25th for the GRS time series in Table 3). Apart from the larger commission errors, patterns of detected burned area were similar for the two processing chains (Figure 7).

Table 2: Acquisition dates for Sentinel 1 (MGRS 20LQQ) and Landsat 8 (Path/Row 230/066)

Sentinel-1 acquisition dates		Landsat 8 acquisition dates	
22.04.2016	20.08.2016*	01.05.2016	05.08.2016
16.05.2016	25.09.2016	18.06.2016	06.09.2016
09.06.2016	7.10.2016	04.07.2016	22.09.2016
03.07.2016	19.10.2016	20.07.2016	

*not processed within the GRS chain

Table 3: Map accuracy as a function of Sentinel-1 pre-processing chain.

Reference BA from Landsat 8 gap filled with Sentinel-2						MGRS tile
Processed at 50 m by GRS*			Processed at 50 m by OTB			
OA	OE	CE	OA	OE	CE	20LQQ
0.943	0.64	0.75	0.973	0.57	0.36	

*the considerably larger CE errors when using GRS processed data is likely related to the reduced number of available dates which allowed for larger than one-month gaps between Sentinel-1 datasets.

(a)

(b)

(c)
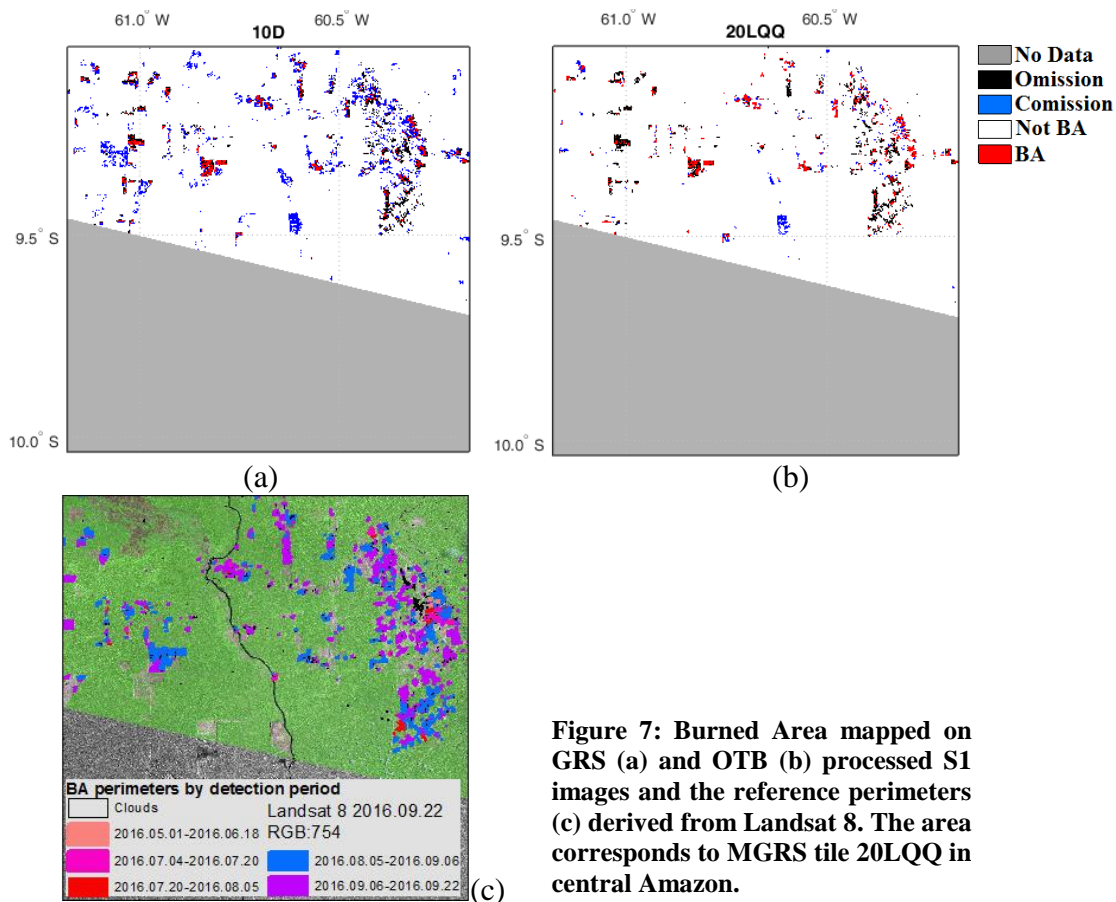
Figure 7: Burned Area mapped on GRS (a) and OTB (b) processed S1 images and the reference perimeters (c) derived from Landsat 8. The area corresponds to MGRS tile 20LQQ in central Amazon.

6   BA performance and preliminary validation

The preliminary validation of the BA algorithm described in [RD-2] was carried out for temporally filtered images processed at 40 m spatial resolution as the agreement between burned area detected from optical and respectively radar sensors over similar periods (Table 4). Results (Table 5) are provided for all tiles used during algorithm calibration and the independent validation except one (18NYK). For tile 18NYK, the Sentinel-1 data could not be processed with the OTB chain as the GRD files were not available on the on-line repository anymore. The reference BA was mapped using the BAMS software and Landsat 8 datasets as described in [RD-2]. Temporal gaps caused by cloud presence during Landsat 8 acquisition were filled using Sentinel-2 images. In such cases, the BA was manually digitized on screen using ArcGIS software. The performance (i.e. in term

of computational speed and spatial resolution) was tested using data processed with the OTB pre-processing chain at two different spatial resolutions (20 and 40 m).

The algorithm works well in most of the studied MGRS tiles with the highest disagreement from the optical derived reference burned areas being observed for the tile 20LQQ, where the CE and OE are somewhat higher when compared to the remaining tiles (Table 5 and Figure 8). This may be explained by decorrelation processes between fire date detection date (date when backscatter is at its minimum) and the actual fire date. This phenomenon seems to affect particularly tile 20LQQ. Although, the BA detection algorithm is designed to deal to such temporal decorrelation effects, its success is not certain particularly when decorrelation processes are characterized by long times. Future versions of the algorithm shall further optimize the reduction of temporal decorrelation errors as more information on when and how such processes happen is gained.

Table 4: Correspondence between BA validation and detection periods.

| Validation period	Detection period	MGRS tile
30.10.2016-02.03.2017	03.11.2016-03.03.2017	18NXG**
30.06.2016-04.10.2016	06.07.2016-28.09.2016	19LGL**
20.07.2016-22.09.2016	03.07.2016-25.09.2016	20LQP***
04.07.2016-22.09.2016	03.07.2016-25.09.2016	20LQQ**
04.07.2016 -25.09.2016	03.07.2016-25.09.2016	20LQR***

Tile type: ** validation, *** algorithm calibration

Table 5: Agreement of the detected BAs with references from optical sensors

Reference BA from: Landsat 8 gap filled with Sentinel-2			Reference BA from: Landsat 8			MGRS tile
OA	OE	CE	OA	OE	CE	
0.993	0.31	0.26	0.992	0.27	0.56	18NXG**
0.999	0.07	0.47	0.999	0.00	0.69	19LGL**
0.997	0.12	0.16	0.997	0.13	0.19	20LQP***
0.972	0.56	0.40	0.972	0.56	0.40	20LQQ**
0.998	0.32	0.20	0.997	0.35	0.20	20LQR***
0.993	**0.37**	**0.28**	**0.992**	**0.38**	**0.38**	**Total**

Tile type: ** validation, *** algorithm calibration

Temporal gap filling using Sentinel-2 data improved the agreement between the reference and detected burned areas by reducing the commission errors (Table 5). The reduction was explained by a more temporally consistent reference dataset which does not miss burned areas characterized by a rapid recovery of greenness. Applying the burned area algorithm to datasets processed at higher spatial resolution (20 m) resulted in identical overall map accuracies when compared to using 40 m spatial resolution images (Table 6). Mixed results were observed for OE and CE when increasing the spatial resolution of the input Sentinel 1 datasets, with CE seemingly increasing (6%) most likely due to higher speckle at 20 m spatial resolution. The difference in OE between 20 and 40 m products were low (2-3%) and of different signs for the two tiles analyzed (Table 6). The different sign can be related with the small values observed. The BA algorithm processing speed

over 20 m spatial resolution tiles increased tenfold to about 10 hours per tile which is explained by the four time increase in the number of pixels to process and the snowballing effect on the selection of training pixels, classification, and post-classification operations.
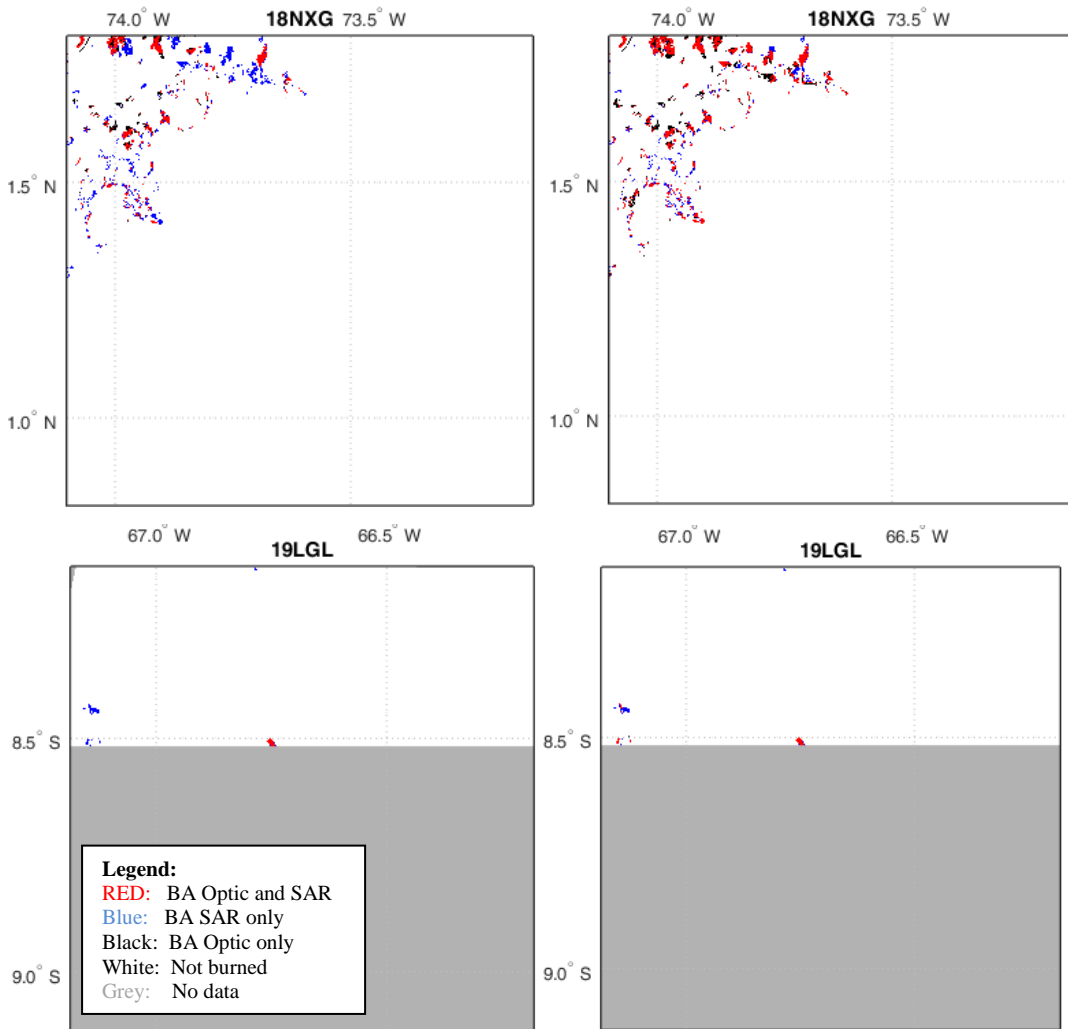
Figure 8: Agreement of detected BA with the reference BA derived from Landsat 8 (left panels) and Landsat 8 gap filled with Sentinel-2 (right panels). Examples of the validation tiles from the Amazon basin.

Table 6: Observed accuracy metrics (OA, OE, CE) and processing time by spatial resolution

Reference BA from Landsat 8 gap filled with Sentinel-2								MGRS tile
Processed at 20 m spatial resolution				Processed at 40 m spatial resolution				
OA	OE	CE	Speed (min)	OA	OE	CE	Speed (min)	
0.993	0.28	0.33	669.45	0.993	0.31	0.26	64.79	18NXG**
0.998	0.34	0.26	598.10	0.998	0.32	0.20	83.58	20LQR***

Tile type: ** validation, *** algorithm calibration

7   References

Anfinsen, S.N., Doulgeris, A.P., & Eltoft, T. (2009). Estimation of the Equivalent Number of Looks in Polarimetric Synthetic Aperture Radar Imagery. *IEEE Transactions on Geoscience and Remote Sensing, 47*, 3795-3809

Boschetti, L., Flasse, S.p.P., & Brivio, P.A. (2004). Analysis of the conflict between omission and commission in low spatial resolution dichotomic thematic products: The Pareto Boundary. *Remote Sensing of Environment, 91*, 280-292

Boschetti, L., Stehman, S.V., & Roy, D.P. (2016). A stratified random sampling design in space and time for regional to global scale burned area product validation. *Remote Sensing of Environment, 186*, 465-478

Chuvieco, E., Opazo, S., Sione, W., Del Valle, H., Anaya, J., Di Bella, C., Cruz, I., Manzo, L., López, G., Mari, N., González-Alonso, F., Morelli, F., Setzer, A., Csiszar, I., Kanpandegi, J.A., Bastarrika, A., & Libonati, R. (2008). Global Burned Land Estimation in Latin America using MODIS Composite Data. *Ecological Applications, 18*, 64-79

Frey, O., Santoro, M., Werner, C.L., & Wegmüller, U. (2013). DEM-Based SAR Pixel-Area Estimation for Enhanced Geocoding Refinement and Radiometric Normalization. *Geoscience and Remote Sensing Letters, IEEE, 10*, 48-52

Giglio, L., Loboda, T., Roy, D.P., Quayle, B., & Justice, C.O. (2009). An active-fire based burned area mapping algorithm for the MODIS sensor. *Remote Sensing of Environment, 113*, 408-420

Padilla, M., Olofsson, P., Stephen V., S., Tansey, K., & Chuvieco, E. (2017). Stratification and sample allocation for reference burned area data. *Remote Sensing of Environment, in press*

Padilla, M., Stehman, S.V., Litago, J., & Chuvieco, E. (2014). Assessing the temporal stability of the accuracy of a time series of burned area products. *Remote Sensing, 6*, 2050-2068

Quegan, S., Toan, T.L., Yu, J.J., Ribbes, F., & Floury, N. (2000). Multitemporal ERS SAR Analysis Applied to Forest Mapping. *IEEE Transactions on Geoscience and Remote Sensing, 38*, 741-752

Roy, D.P., & Boschetti, L. (2009). Southern Africa validation of the MODIS, L3JRC, and GlobCarbon burned-area products. *IEEE Transactions on Geoscience and Remote Sensing, 47*, 1032-1044

Schubert, A., Small, D., Miranda, N., Geudtner, D., & Meier, E. (2015). Sentinel-1A Product Geolocation Accuracy: Commissioning Phase Results. *Remote Sensing, 7*, 9431-9449

Tanase, M., Ismail, I., Lowell, K., Karyanto, O., & Santoro, M. (2015). Detecting and quantifying forest change: the potential of existing C- and X-band radar datase. *PLOS ONE, 10(6): e0131079*, 1-14

Wegmüller, U., Werner, C., Strozzi, T., & Wiesmann, A. (2002). Automated and precise image registration procedures. In L. Bruzzone, & P. Smits (Eds.), *Analysis of multi-temporal remote sensing images* (pp. 37-49). Singapore: World Scientific 2002

Werner, C., Wegmuller, U., Strozzi, T., & Wiesmann, A. (2005). Precision estimation of local offsets between pairs of SAR SLCs and detected SAR images. In, *Geoscience and Remote Sensing Symposium* (pp. 4803 - 4805). Seoul: IEEE

Annex 1: Acronyms and abbreviations

ATBD	Algorithm Theoretical Basis Document
BA	Burned Area
BAMS	Burned Area Mapping Software
CE	Commission error
CESBIO	Centre of the Study of the Biosphere from Space
DEM	Digital Elevation Model
ENL	Equivalent number of looks
GPL	General Public License
GRD	Ground Range Detected
GRS	Gamma Remote Sensing
LDA	Large Area Demonstrator
MGRS	Military Grid Reference System
MLI	Multi-Looked Image
MTF	Multi-Temporal Filtering
OA	Overall Accuracy
OE	Omission error
OTB	Orfeo ToolBox
PEPS	Plateforme d'Exploitation des Produits Sentinel
POD	Precise Orbit Determination
RD	Reference Document
RSS	Remote Sensing Solutions GmbH
S-1	Sentinel 1
SAR	Synthetic Aperture Radar
SFD	Small Fires Dataset
SRTM	Shuttle Radar Topography Mission